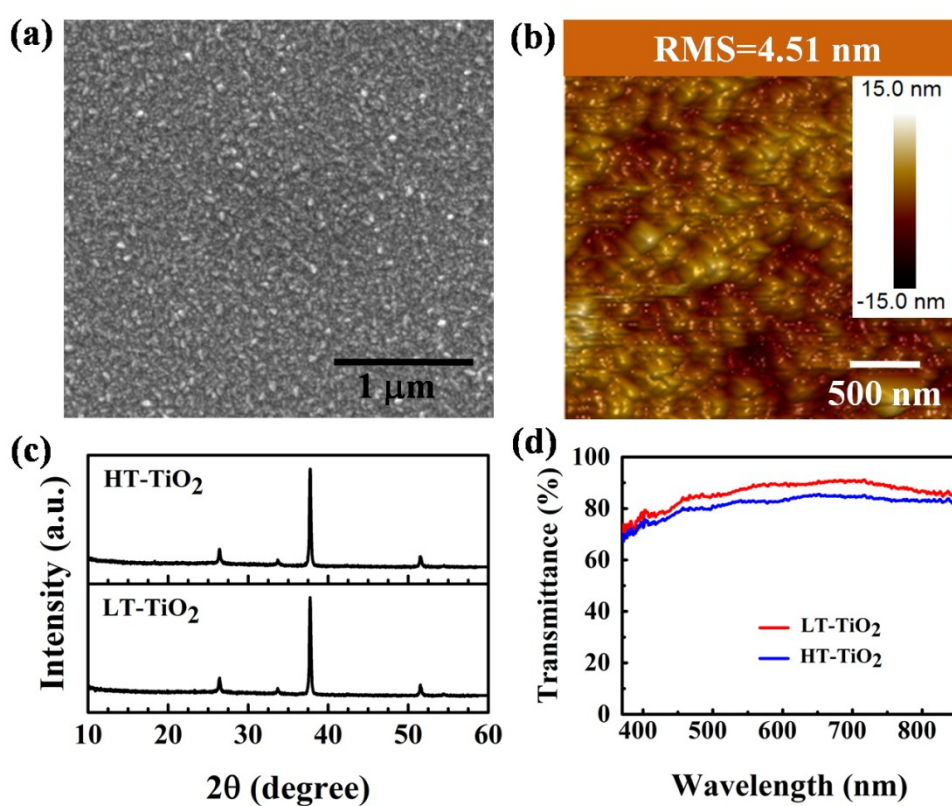


*Supporting Information*

## Highly Efficient Flexible Solar Cells Based on Room-Temperature Processed Inorganic Perovskite

Yanqiang Hu<sup>a</sup>, Shufang Zhang<sup>a\*</sup>, Ting Shu<sup>b</sup>, Ting Qiu<sup>a</sup>, Fan Bai<sup>a</sup>, Wei Ruan<sup>a</sup>, Feng Xu<sup>a\*</sup>

This file includes **Figure S1-S18** and **Table S1-S6**:



**Figure S1.** (a) SEM image and (b) AFM image of the low-temperature processed TiO<sub>2</sub> compact layer on ITO-PET substrate. (c) XRD spectra and (d) optical transmittance spectra of as synthesized low-temperature (LT) and high-temperature (HT) TiO<sub>2</sub> compact layer on ITO-glass substrate, respectively.

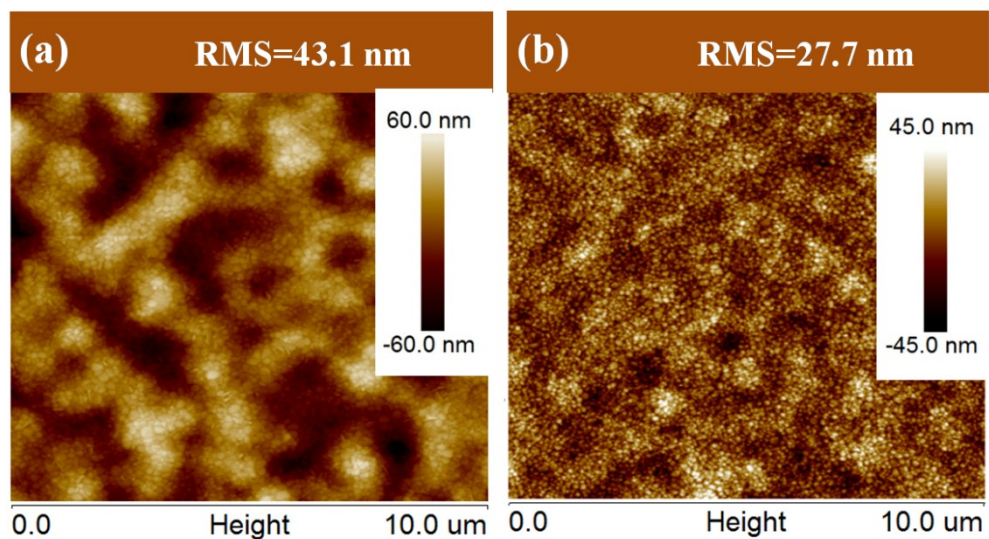


**Figure S2.** AFM images of (a) A-CsPb<sub>0.96</sub>Bi<sub>0.04</sub>I<sub>3</sub> film and (b) RT-CsPb<sub>0.96</sub>Bi<sub>0.04</sub>I<sub>3</sub> film on flexible PET substrate, respectively.

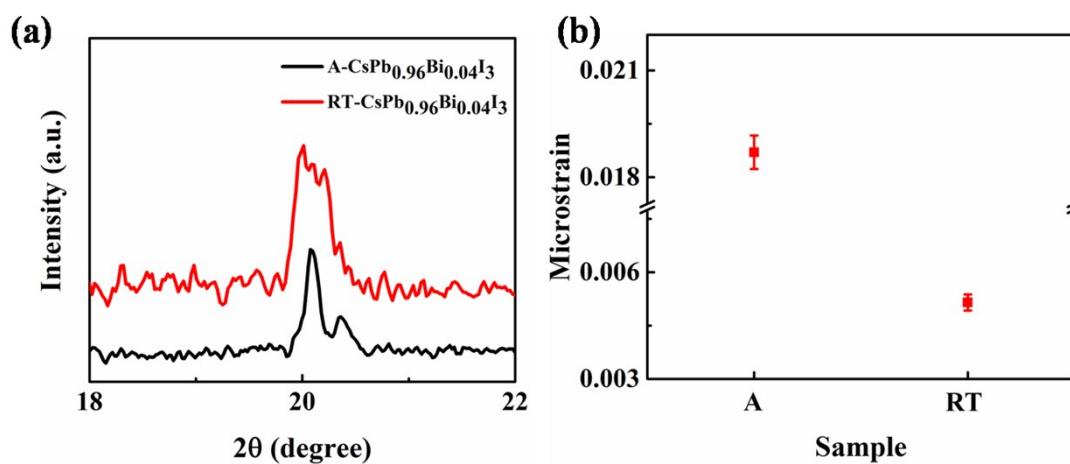


**Figure S3.** (a) XRD patterns of A-CsPb<sub>0.96</sub>Bi<sub>0.04</sub>I<sub>3</sub> and RT-CsPb<sub>0.96</sub>Bi<sub>0.04</sub>I<sub>3</sub> perovskite films. (b) Calculated microstrain in the A-CsPb<sub>0.96</sub>Bi<sub>0.04</sub>I<sub>3</sub> and RT-CsPb<sub>0.96</sub>Bi<sub>0.04</sub>I<sub>3</sub> perovskite films from XRD patterns.

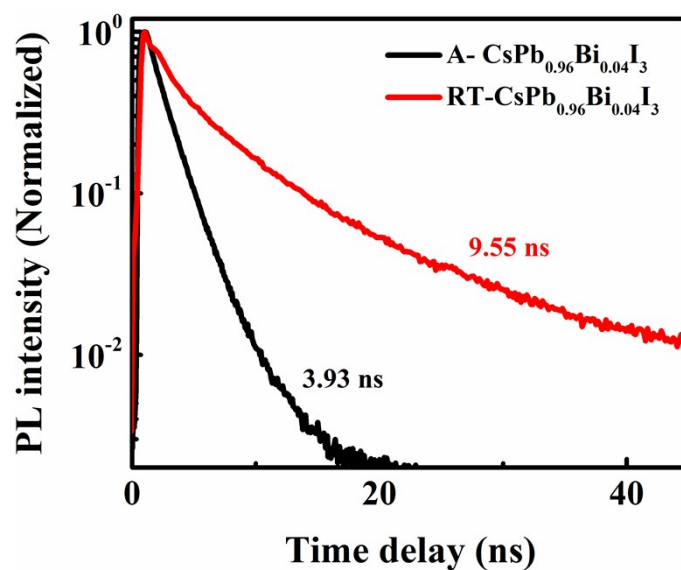


**Figure S4.** Time-resolved PL spectra of the A-CsPb<sub>0.96</sub>Bi<sub>0.04</sub>I<sub>3</sub> and RT-CsPb<sub>0.96</sub>Bi<sub>0.04</sub>I<sub>3</sub> films deposited on glass substrate with excitation wavelength at 460 nm, respectively.

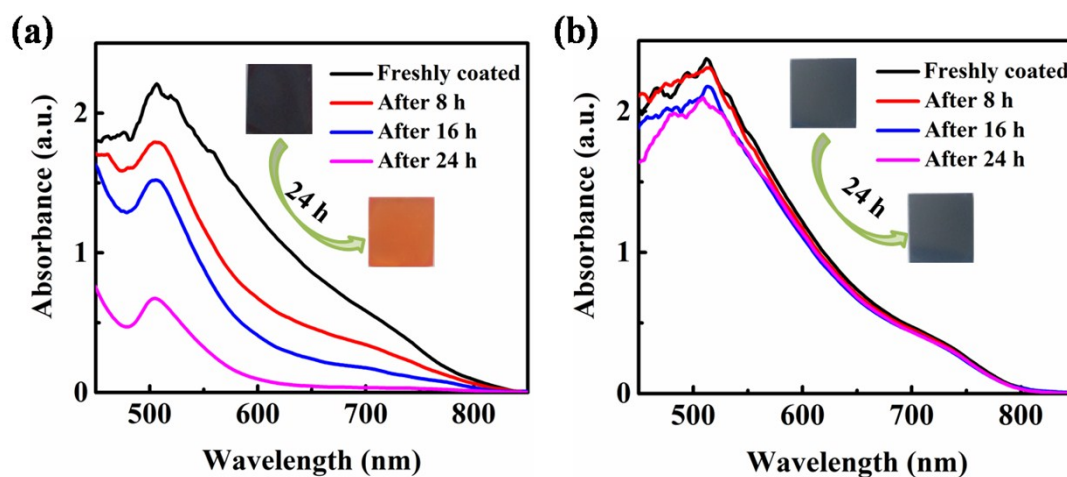


**Figure S5.** Change of UV-vis spectra with different exposure time of freshly-prepared (a) A-CsPb<sub>0.96</sub>Bi<sub>0.04</sub>I<sub>3</sub> and (b) RT-CsPb<sub>0.96</sub>Bi<sub>0.04</sub>I<sub>3</sub> films.

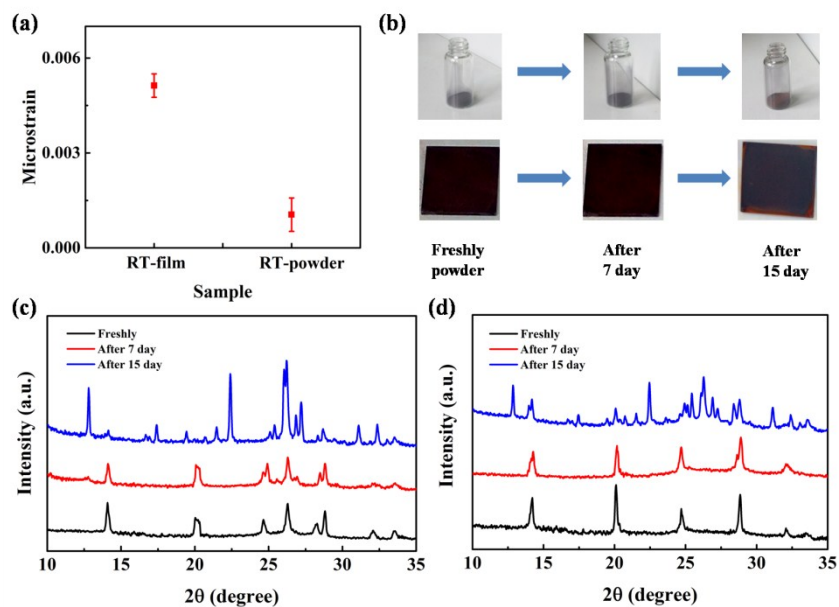


**Figure S6.** (a) Calculated microstrains of the cubic  $\text{RT-Cspb}_{0.96}\text{Bi}_{0.04}\text{I}_3$  films (RT-film) and the corresponding scraped powder (RT-powder), respectively. (b) Photographs of the cubic  $\text{RT-Cspb}_{0.96}\text{Bi}_{0.04}\text{I}_3$  films and the corresponding scraped powder freshly and exposed in 50% RH condition for 7 day and 15 day under dark. Change of XRD with time of (c) the cubic  $\text{RT-Cspb}_{0.96}\text{Bi}_{0.04}\text{I}_3$  film, and (d) the corresponding scraped powder of  $\text{RT-Cspb}_{0.96}\text{Bi}_{0.04}\text{I}_3$ .

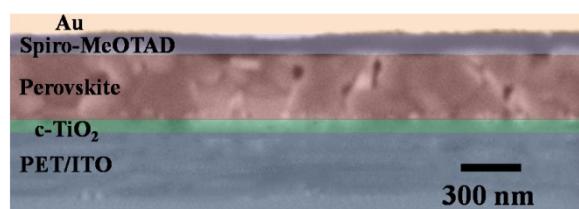


**Figure S7.** Cross-sectional SEM image of a solar cell based on the  $\text{A-Cspb}_{0.96}\text{Bi}_{0.04}\text{I}_3$  film.

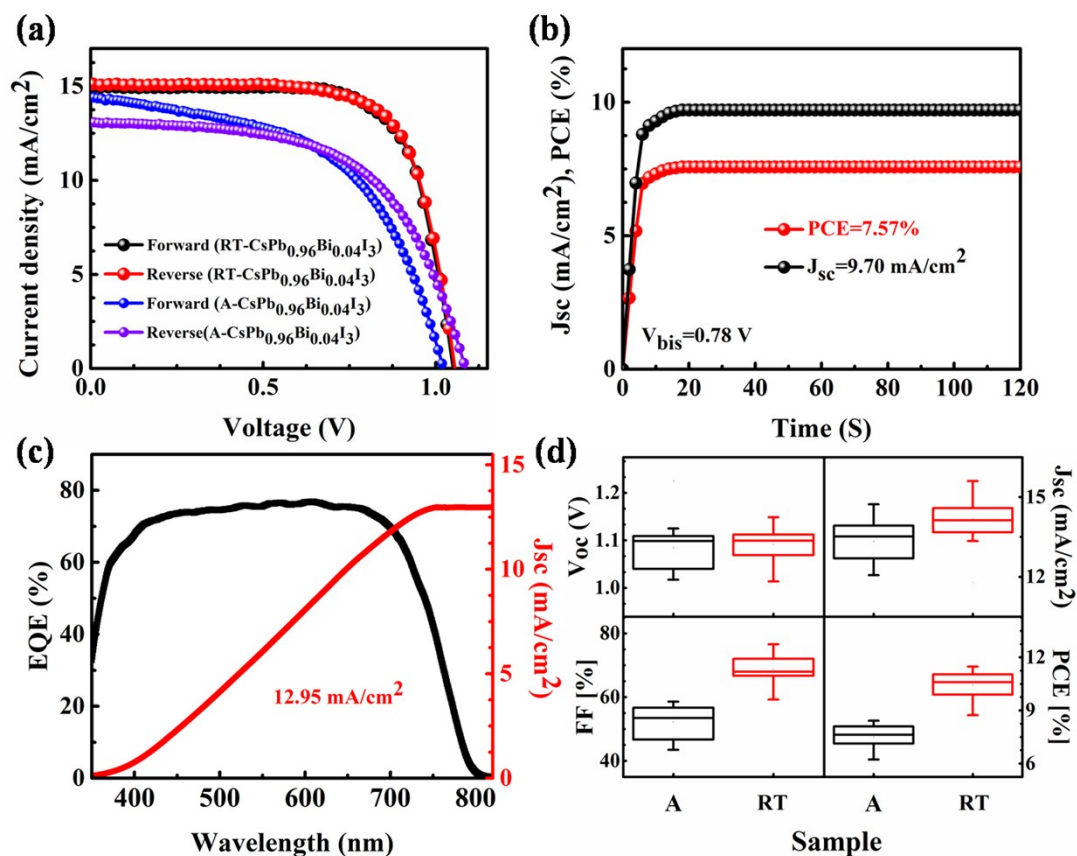


**Figure S8.** (a)  $J$ - $V$  characteristics of the best-performing device achieved with A-CSPb<sub>0.96</sub>Bi<sub>0.04</sub>I<sub>3</sub> and RT-CSPb<sub>0.96</sub>Bi<sub>0.04</sub>I<sub>3</sub> film. The  $J$ - $V$  characteristics were obtained by both forward and reverse scanning direction with scanning rate of 0.1 V/s. (b) Steady-state photocurrent output at the maximum power point (0.78V) of the best-performing A-CSPb<sub>0.96</sub>Bi<sub>0.04</sub>I<sub>3</sub> device. (c) External quantum efficiency (EQE) spectrum and integrated  $J_{sc}$  spectra of the champion flexible A-CSPb<sub>0.96</sub>Bi<sub>0.04</sub>I<sub>3</sub> device. (d) Photovoltaic parameter statistics of the solar cells based on A-CSPb<sub>0.96</sub>Bi<sub>0.04</sub>I<sub>3</sub> and RT-CSPb<sub>0.96</sub>Bi<sub>0.04</sub>I<sub>3</sub> films.

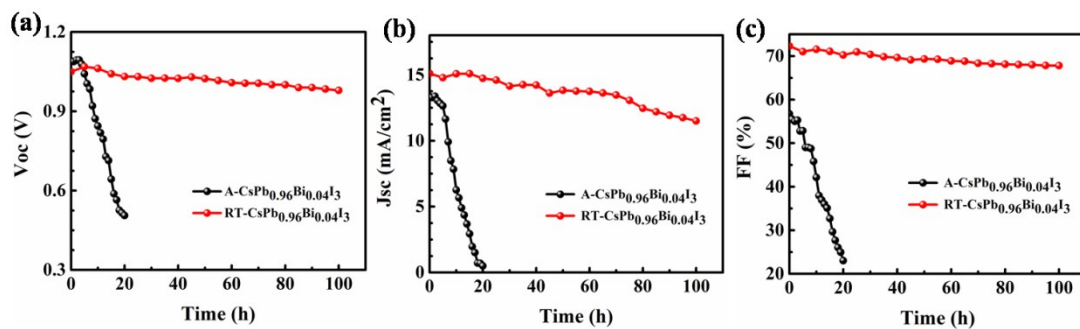


**Figure S9.**  $V_{oc}$ ,  $J_{sc}$  and FF of the best-performing devices prepared using A-CSPb<sub>0.96</sub>Bi<sub>0.04</sub>I<sub>3</sub> and RT-CSPb<sub>0.96</sub>Bi<sub>0.04</sub>I<sub>3</sub> films, as a function of time.

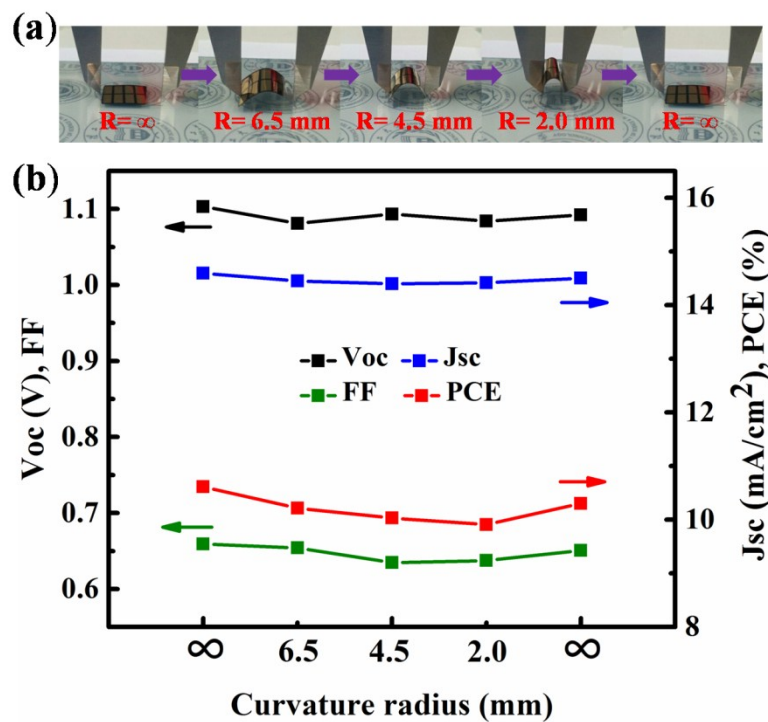


**Figure S10.** (a) Photographs of the flexible RT-CsPb<sub>0.96</sub>Bi<sub>0.04</sub>I<sub>3</sub> device at curvature radii from  $\infty$  to 2.0 mm. (b) The variation of Voc, Jsc, FF and PCE versus curvature radii for the flexible cells based on RT-CsPb<sub>0.96</sub>Bi<sub>0.04</sub>I<sub>3</sub> film.

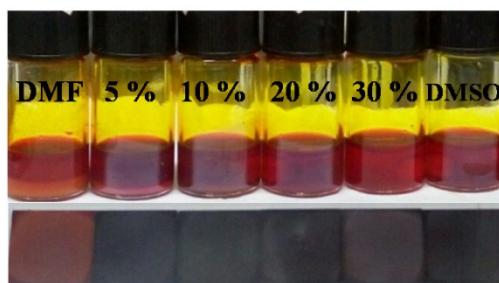


**Figure S11.** Photographs of the perovskite precursor solutions and corresponding films with different DMSO concentration.

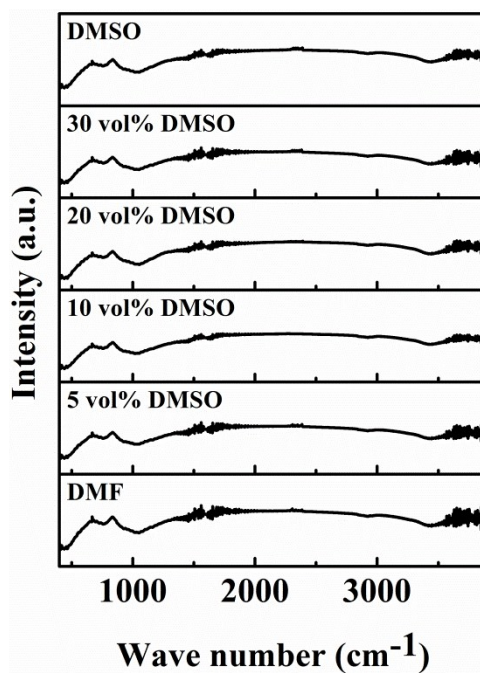


**Figure S12.** Infrared (IR) spectra of RT-CsPb<sub>0.96</sub>Bi<sub>0.04</sub>I<sub>3</sub> films prepared from precursor solutions in DMF with increasing volume fractions of DMSO.

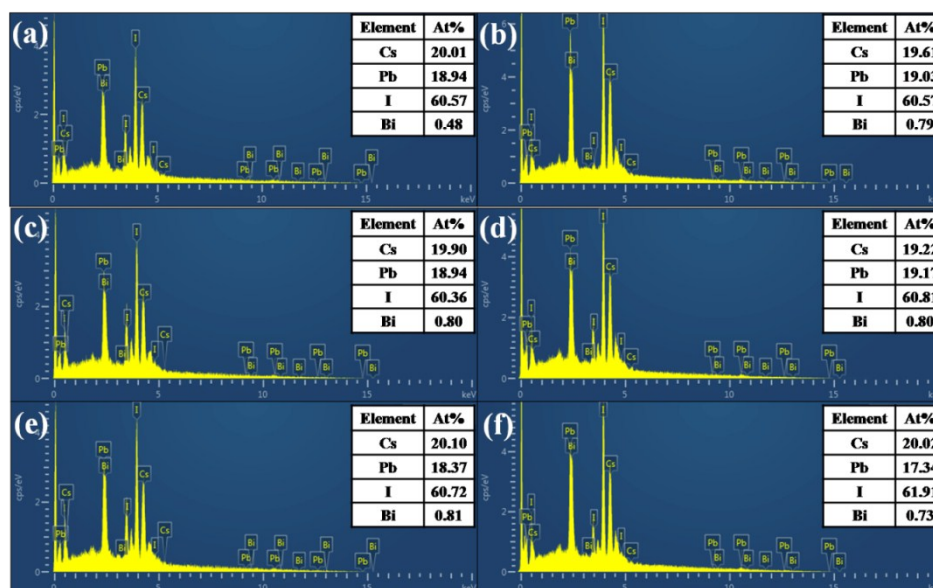


**Figure S13.** EDS results of RT-CsPb<sub>0.96</sub>Bi<sub>0.04</sub>I<sub>3</sub> films prepared from precursor solutions in DMF with increasing volume fractions of DMSO. (a) pure DMF; (b) 5 vol % DMSO; (c) 10 vol % DMSO; (d) 20 vol % DMSO; (e) 30 vol % DMSO; and (f) pure DMSO.

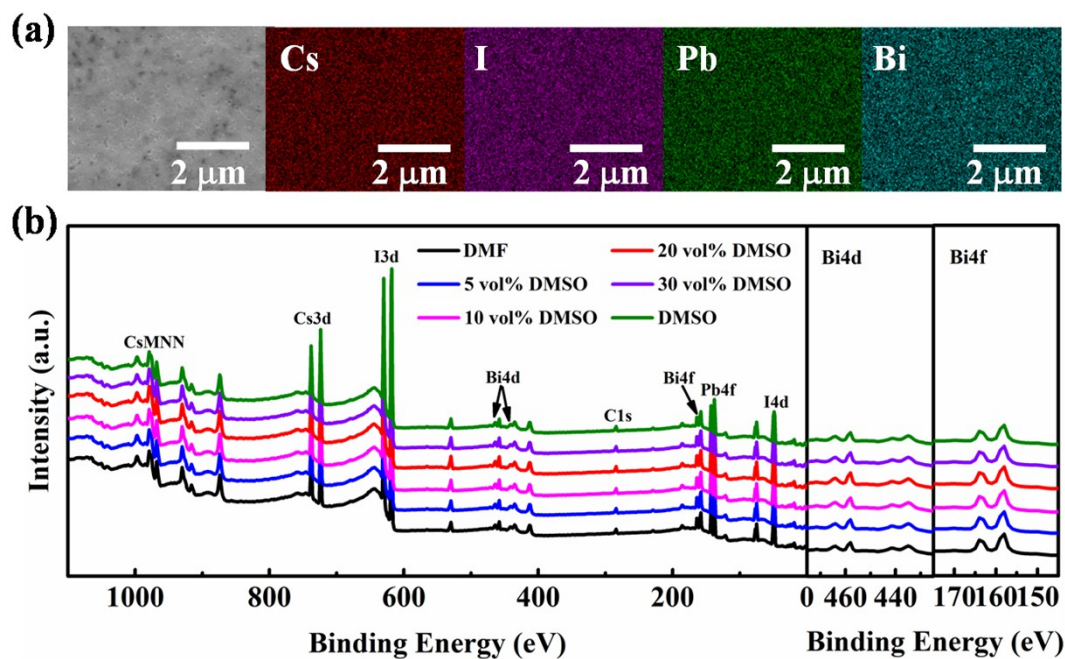


**Figure S14.** (a) Energy dispersive X-ray spectroscopy (EDS) mapping of RT-CsPb<sub>0.96</sub>Bi<sub>0.04</sub>I<sub>3</sub> films prepared from precursor solutions with 20 vol% DMSO in the mixed solvent. (b) Overview XPS spectra of RT-CsPb<sub>0.96</sub>Bi<sub>0.04</sub>I<sub>3</sub> films prepared from precursor solutions with increasing volume fractions of DMSO in the mixed solvent.

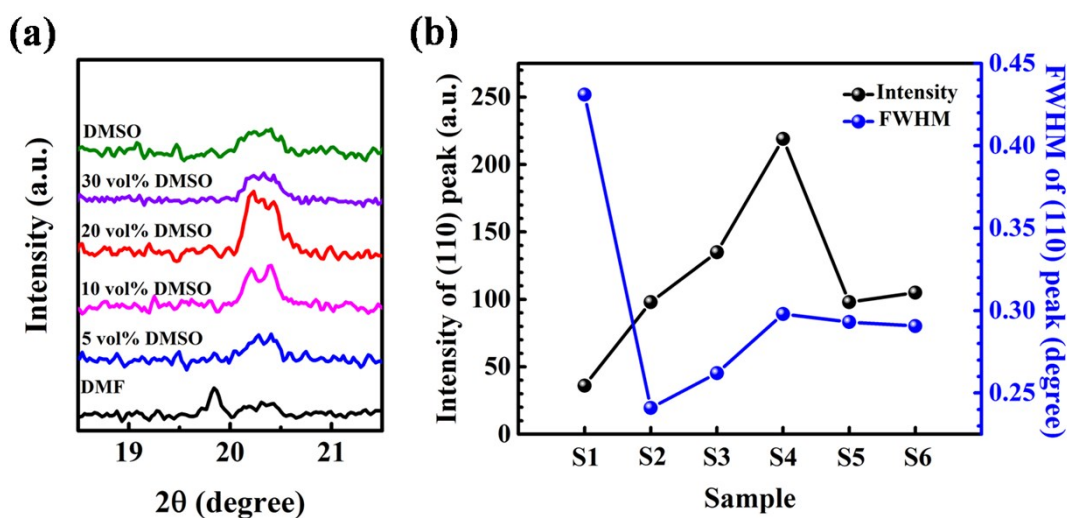


**Figure S15.** (a) XRD patterns of RT-CsPb<sub>0.96</sub>Bi<sub>0.04</sub>I<sub>3</sub> films prepared from precursor solutions in DMF with increasing volume fractions of DMSO. (b) Intensity and FWHM variations of (110) peak of RT-CsPb<sub>0.96</sub>Bi<sub>0.04</sub>I<sub>3</sub> films prepared from precursor solutions in DMF with increasing volume fractions of DMSO. (S1) pure DMF, (S2) 5 vol % DMSO, (S3) 10 vol % DMSO, (S4) 20 vol % DMSO, (S5) 30 vol % DMSO, and (S6) pure DMSO.

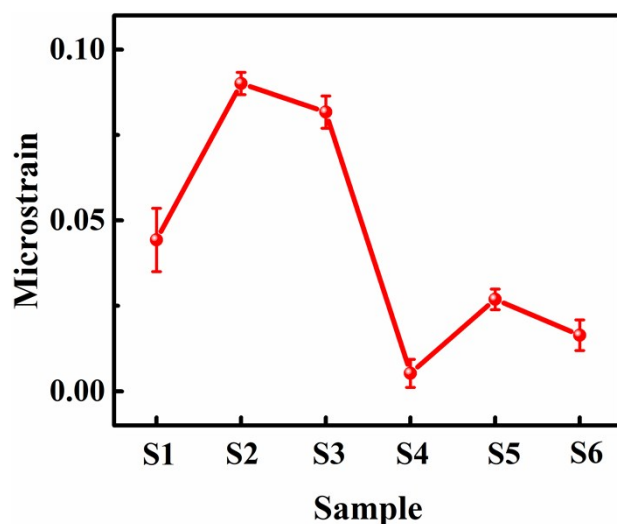


**Figure S16.** Calculated microstrains with error bars of RT-CsPb<sub>0.96</sub>Bi<sub>0.04</sub>I<sub>3</sub> films prepared from precursor solutions in DMF with increasing volume fractions of DMSO. (S1) pure DMF, (S2) 5 vol % DMSO, (S3) 10 vol % DMSO, (S4) 20 vol % DMSO, (S5) 30 vol % DMSO, and (S6) pure DMSO.

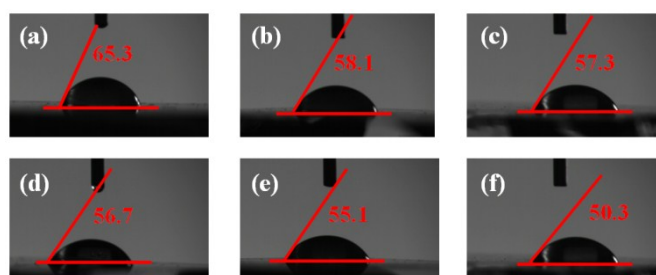


**Figure S17.** Contact angles between PET substrate and the perovskite precursor solutions with different solvent: (a) pure DMF, (b) 5 vol % DMSO, (c) 10 vol % DMSO, (d) 20 vol % DMSO, (e) 30 vol % DMSO, and (f) pure DMSO.

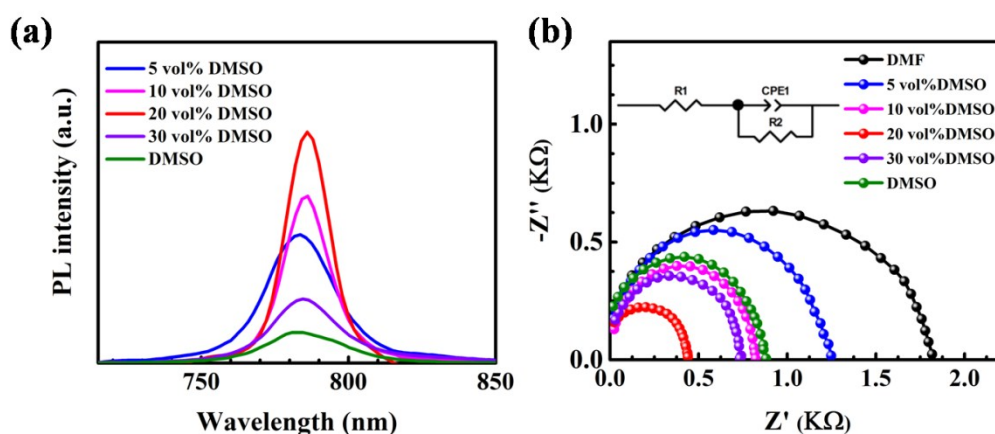


**Figure S18.** (a) Normalized PL of the RT-CsPb<sub>0.96</sub>Bi<sub>0.04</sub>I<sub>3</sub> films prepared with different concentration of DMSO in the mixed solvent. (b) Nyquist plots of the PET/ITO/c-TiO<sub>2</sub>/Perovskite/Au device based on the RT-CsPb<sub>0.96</sub>Bi<sub>0.04</sub>I<sub>3</sub> prepared with different concentration of DMSO in the mixed solvent. The measured results were shown as dots while the fitted results shown as solid lines. The inset in (b) was equivalent circuit model.

**Table S1** Intensity and FWHM variations of (110) peak and corresponding calculated grain size and average microstrain of RT-CsPb<sub>0.96</sub>Bi<sub>0.04</sub>I<sub>3</sub> and A-CsPb<sub>0.96</sub>Bi<sub>0.04</sub>I<sub>3</sub> film.

Sample	Intensity of(110)	FWHM of(110)	Grain Size (nm)	Microstrain
RT-CsPb <sub>0.96</sub> Bi <sub>0.04</sub> I <sub>3</sub>	219	0.298	65.8	-0.00525
A-CsPb <sub>0.96</sub> Bi <sub>0.04</sub> I <sub>3</sub>	141	0.191	192.2	-0.01807

**Table S2** The extracted equivalent circuit element parameters of the devices based on RT-CsPb<sub>0.96</sub>Bi<sub>0.04</sub>I<sub>3</sub> and A-CsPb<sub>0.96</sub>Bi<sub>0.04</sub>I<sub>3</sub> film, respectively.

Sample	R <sub>s</sub> (Ω)	R <sub>ct</sub> (Ω)	R <sub>rec</sub> (Ω)
RT-CsPb <sub>0.96</sub> Bi <sub>0.04</sub> I <sub>3</sub>	10.576	116.860	676.613
A-CsPb <sub>0.96</sub> Bi <sub>0.04</sub> I <sub>3</sub>	10.881	155.923	569.871

**Table S3** Photovoltaic parameters of the best-performance solar cell based on RT-CsPb<sub>0.96</sub>Bi<sub>0.04</sub>I<sub>3</sub> and A-CsPb<sub>0.96</sub>Bi<sub>0.04</sub>I<sub>3</sub> film measured with forward and reverse scan at 0.1 V/s scan rate, respectively.

Sample	Scan direction	V <sub>OC</sub> [V]	J <sub>SC</sub> [mA cm <sup>-2</sup> ]	FF [%]	PCE [%]
RT-CsPb <sub>0.96</sub> Bi <sub>0.04</sub> I <sub>3</sub>	Forward	1.04	14.93	73.05	11.34
	Reverse	1.05	15.11	72.32	11.47
A-CsPb <sub>0.96</sub> Bi <sub>0.04</sub> I <sub>3</sub>	Forward	1.02	14.40	53.58	7.87
	Reverse	1.09	13.37	56.75	8.27

**Table S4** The atomic percentages of elements in the RT-CsPb<sub>0.96</sub>Bi<sub>0.04</sub>I<sub>3</sub> films extracted from XPS spectra.

	DMF	5 vol% DMSO	10 vol% DMSO	20 vol% DMSO	30 vol% DMSO	DMSO
Cs	19.96	20.01	19.93	19.59	20.10	19.99
Pb	18.89	19.02	18.97	19.54	18.57	18.54
I	60.64	60.16	60.32	60.04	60.48	60.76
Bi	0.51	0.81	0.78	0.83	0.85	0.71

**Table S5** The extracted equivalent circuit element parameters of the RT-CsPb<sub>0.96</sub>Bi<sub>0.04</sub>I<sub>3</sub> device.

	DMF	5 vol% DMSO	10 vol% DMSO	20 vol% DMSO	30 vol% DMSO	DMSO
$R_s$ (K $\Omega$ )	0.0206	0.0176	0.0235	0.0224	0.0300	0.0171
$R_{ct}$ (K $\Omega$ )	1.8171	1.2476	0.8224	0.4394	0.7789	0.8806

**Table S6** Photovoltaic parameters of solar cell devices based on the series of RT-CsPb<sub>0.96</sub>Bi<sub>0.04</sub>I<sub>3</sub> films.

Sample	$V_{oc}$ [V]	$J_{sc}$ [mA cm <sup>-2</sup> ]	$FF$ [%]	$PCE$ [%]
DMF	1.06	3.79	43.06	1.73
5 vol% DMSO	1.10	13.96	56.72	8.71
10 vol% DMSO	1.08	14.53	63.45	9.96
20 vol% DMSO	1.05	15.11	72.32	11.47
30 vol% DMSO	0.98	12.71	61.90	7.71
DMSO	1.01	10.03	54.59	5.53